Journal of Glaciology, Vol. 47, No. 159, 2001

Surface properties and processes of perennial Antarctic sea ice in summer

Christian Haas,[1] David N. Thomas,[2] Jörg Bareiss[3]
[1]*Alfred Wegener Institute for Polar and Marine Research, Columbusstrasse, P.O. Box 120161, D-27568 Bremerhaven, Germany*
[2]*School of Ocean Sciences, University of Wales Bangor, Menai Bridge, Anglesey LL59 5EY, Wales*
[3]*Department of Climatology, Faculty of Geography/Geosciences, University of Trier, D-54286 Trier, Germany*

ABSTRACT. Ice-core and snow data from the Amundsen, Bellingshausen and Weddell Seas, Antarctica, show that the formation of superimposed ice and the development of seawater-filled gap layers with high algal standing stocks is typical of the perennial sea ice in summer. The coarse-grained and dense snow had salinities mostly below 0.1‰. A layer of fresh superimposed ice had a mean thickness of 0.04–0.12 m. Gap layers 0.04–0.08 m thick extended downwards from 0.02 to 0.14 m below the water level. These gaps were populated by diatom standing stocks up to 439 μg L^{-1} chlorophyll *a*. We propose a comprehensive heuristic model of summer processes, where warming and the reversal of temperature gradients cause major transformations in snow and ice properties. The warming also causes the reopening of incompletely frozen slush layers caused by flood–freeze cycles during winter. Alternatively, superimposed ice forms at the cold interface between snow and slush in the case of flooding with negative freeboard. Combined, these explain the initial formation of gap layers by abiotic means alone. The upward growth of superimposed ice above the water level competes with a steady submergence of floes due to bottom and internal melting and accumulation of snow.

1. INTRODUCTION

Sea ice in the Southern Ocean extends from a summer minimum of about 4×10^6 km^2 in March to a winter maximum of about 20×10^6 km^2 in October (Gloersen and others, 1992). This strong seasonal variability has impacts on processes and interactions in the ocean, atmosphere and the marine biosphere. The rapid sea-ice formation in winter is well understood, and occasionally referred to as the "pancake cycle" (Lange and others, 1989): in the turbulent supercooled waters of the marginal sea-ice zone, frazil ice forms and subsequently consolidates into pancake ice. The pancakes grow further by rafting and ad-freezing, and aggregate into larger ice floes. The frazil origin of most sea ice in Antarctica is reflected in its fine orbicular granular crystal texture (Eicken and Lange, 1989), typical of the majority of ice cores drilled in the Weddell Sea (Gow and others, 1987; Drinkwater and Haas, 1994; Eicken, 1998), the Bellingshausen, Amundsen and Ross Seas (Jeffries and Weeks, 1993; Jeffries and others, 1997) and in East Antarctica (Worby and others, 1998). Once the ice cover is closed and waves are absent, freezing takes place in open leads or underneath the floes primarily by congelation. These ice types are generally marked by a columnar crystal texture.

A further notable and widespread process of Antarctic sea-ice formation is the freezing of snow slush at the snow/ice interface after surface flooding. A thick snow cover depresses the ice surface below the water level, such that sea water floods the ice surface and subsequently refreezes together with the water-saturated snow. This process is referred to as "flood–freeze cycling" (Fritsen and others, 1998). The resulting "snow ice" has a fine granular texture, too, and can only be distinguished from granular ice of frazil origin by its negative δ^{18}O due to the large meteoric snow fraction (Lange and others, 1990). The contribution of snow ice to the total sea-ice volume may be as large as 25% (Eicken and others, 1994; Jeffries and others, 1997).

The processes described above are most important in the cold season from early fall to late spring, when air temperatures are below the freezing temperature of sea water. In summer, temperature gradients in the ice and snow are frequently zero or even positive. Consequently, most ice deteriorates by bottom and lateral melting due to heating from above and below (Martinson and Iannuzzi, 1998). Before melting completely, the rotten ice becomes extremely porous and develops a honeycomb-like structure. Nevertheless, some sea ice survives the Antarctic summer season, but little is known about its surface processes and properties. Casually, "superimposed ice" has been observed at the snow/ice interface of drifting pack ice (Ackley and others, 1979; Gow and others, 1987; Jeffries and others, 1994; Eicken, 1998), and frequently on fast ice (Kawamura and others, 1993, 1997). This has a large-grained, polygonal granular (PG) texture, and forms as a result of snow metamorphosis during "melt–freeze cycling" (Colbeck, 1997). Single crystals can have diameters of several centimetres, as a result of rapid grain coarsening in wet snow (Colbeck, 1987).

Occasionally, an almost continuous "gap" or high-porosity layer is found at, or just below, the water level, overlain by a thin solid layer of ice. These gap layers host active biological assemblages, providing optimum conditions of light and nutrient replenishment (Kottmeier and Sullivan, 1990; Garrison and Buck, 1991; Ackley and Sullivan, 1994; Fritsen and others, 1994; Lytle and Ackley, 1996). Haas (1998) has inferred that this gap layer is widespread in the Bellingshausen and Amundsen Seas, because the apparent electrical ice conduc-

https://doi.org/10.3189/172756501781831864 Published online by Cambridge University Press

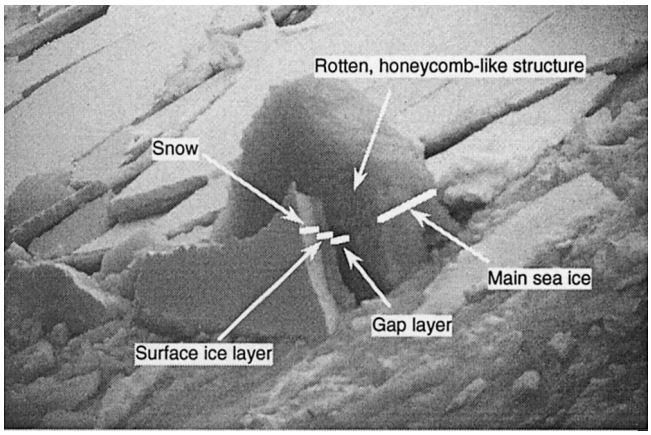

Fig. 1. Photograph of a tilted floe broken by the ship, showing the surface layer, gap and rotten ice structure typically found in summer. Total thickness of the floe is about 1.00 m.

tivity was significantly higher than in other seasons as a result of sea water filling the gaps.

Ackley and others (1979) and Ackley and Sullivan (1994) explain the gap layers, also referred to as "freeboard layers" (Ackley and Sullivan, 1994; Fritsen and others, 1994), as a result of a biophysical feedback process at the onset of summer warming. Due to increased temperatures and the seasonal rise in solar radiation, brine drainage from the ice surface triggers a salinity and nutrient flux to the layer below the surface. There, an algal bloom occurs, increasing radiation absorption due to the dark colour of the algae, leading to further melt and the development of a rotten ice layer. It should be noted here that this mechanism requires thin snow in order to allow for significant radiation transmission, and needs rather high algal standing stocks (Zeebe and others, 1996), as well as a positive ice freeboard.

Here, we report results from comprehensive physical and biological investigations of ice and snow properties of perennial ice in summer 1994 in the Bellingshausen and Amundsen Seas, and in summer 1997 in the Weddell Sea. During both studies, large amounts of superimposed ice as well as numerous surface gap layers were observed. Figure 1 shows a photograph of a floe fragment tilted upright by an ice-breaker. The rotten sea ice with a honeycomb-like upper layer, a surface gap and a solid layer of mostly superimposed ice overlain by snow can be distinguished. We will particularly focus on the ice layer above the gap, which we sampled along horizontal surface profiles with a high vertical resolution. Based on our data, we propose a heuristic model of the various processes at the surface of Antarctic sea ice from the onset of summer melt until the beginning of fall freeze-up. These could provide a link between summer properties and features described in previous studies, as well as alternative explanations for the gap-layer formation. The processes also have profound consequences for remote-sensing studies of Antarctic sea ice in summer.

2. MATERIAL AND METHODS

Snow-property measurements and ice coring were performed during two expeditions of RV *Polarstern* to the Bellingshausen and Amundsen Seas in February 1994 (Haas and Viehoff, 1994; Haas and others, 1996) and to the Weddell Sea in January and February 1997 (Haas and others, 1998). En route, 2 hourly visual ice observations were performed and documented as proposed by Worby and Allison (1999). The locations of the sampled floes, as well as the mean ice coverage in February 1994 and 1997, are shown in Figure 2. In 1997 the ship crossed the Weddell Sea twice along a southeast–northwest transect, covering a wide range of ice regimes. Most floes were visited by helicopter while the ship was underway. In total, 33 floes were sampled in 1997, and 15 in 1994.

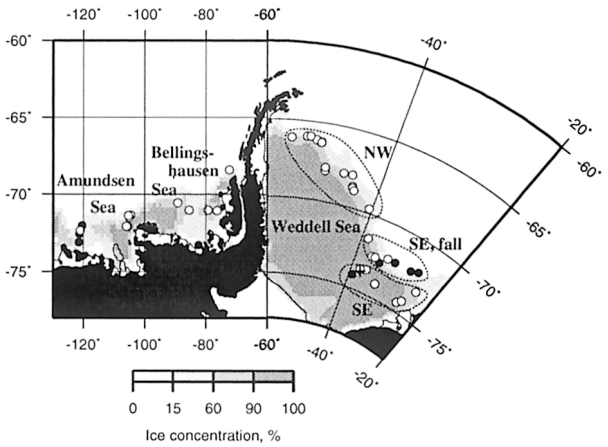

Fig. 2. Map of the research areas in the Amundsen and Bellingshausen Seas and Weddell Sea in 1994 and 1997, respectively, showing the locations of the sampled floes (circles). Open circles indicate floes with PG ice at the snow/ice interface. The mean February ice concentration derived from satellite passive-microwave Special Sensor Microwave/Imager data (provided on CDs by the U.S. National Snow and Ice Data Center, Boulder, Colorado) is also shown for the respective year.

On almost every floe, electromagnetic (EM) ice-thickness measurements were carried out using a Geonics EM31 with 5 m spacing along profiles of 50 to >1000 m length (Haas and others, 1997; Haas, 1998). In 1994, most EM soundings were accompanied by drillhole measurements for validation and to determine the ice freeboard. In 1997, only a few drillhole measurements were carried out and the freeboard was surveyed with a laser levelling device along the EM profiles.

2.1. Snow measurements

Snow thickness was measured with a spacing of 1 m on representative 50–100 m subsections along the ice-thickness profiles with the aid of a ruler stick. Vertical profiles of snow temperature, wetness, density, salinity and grain-size were measured in up to three snow pits. Both thin snow on level ice and thick snow around pressure ridges were sampled. Snow temperature was measured with a Pt-100 thermometer at vertical spacings of 0.05–0.10 m, depending on snow thickness. In parallel, snow wetness was measured with a TOIKKA Snow Fork (Helsinki, Finland). Snow wetness in percentage liquid-water content is calculated from fork resonator measurements of the complex snow permittivity (Shivola and Tiuri, 1986).

After visual examination of the snow stratigraphy, samples were taken from the main layers with 0.05 m diameter, 0.5 L steel tubes. In the cold laboratory on board the ship, snow density was measured by weighing these samples. After visual grain-size estimation using a millimetre grid, the samples were melted and subsequently their salinity was measured with a Wissenschaflich-Technische-Werkstätten GmbH LF181 conductivity meter which was calibrated to

https://doi.org/10.3189/172756501781831864 Published online by Cambridge University Press

display salinity. If the salinity was <0.1‰, the instrument gave a reading of 0.0‰.

2.2. Ice coring and analysis

From each floe, two 0.09 m diameter ice cores were drilled from level ice with a gas-motor-driven Kovacs Enterprise ice auger after the snow had carefully been removed. Such cores are referred to as "main cores". In 1997, the top sections of the cores were drilled mostly by hand until the gap layer was encountered (see below). This "surface core" was retained from the core tube without turning it upside down, to avoid contamination of the ice with sea water and brine. After recovery, the surface cores were stored upright in pre-cooled cold boxes to minimize melting, brine drainage and contamination during the helicopter transport to the ship's cold laboratory (<−25°C). Then cores of the remaining ice were taken and stored horizontally in plastic tubes for transfer to the ship.

The second core was immediately cut into 0.1 m sections and allowed to melt slowly for later chlorophyll-*a* measurements by standard fluorometric procedures (Thomas and others, 1998).

When surface gaps were encountered at the main coring site in 1997, up to four additional surface cores were drilled a few metres apart to determine the extent and abundance of these features. The thicknesses of the ice layers, the gap layers, as well as the freeboard height were measured. Water from the gaps was sampled for salinity. Ice crystals and slush were sieved out using a mesh size of 1 mm^2.

In the cold laboratory, detailed analyses of ice texture were performed on thick and thin sections of the cores (e.g. Lange, 1988). The cores were cut according to stratigraphic units. The surface cores were cut with a high vertical resolution of 0.01–0.03 m. While two-thirds of the segments were subsequently melted for salinity measurements, the rest was transferred to the home laboratory. On a limited number of these samples, ^{18}O concentrations were determined as described by Eicken and others (1994) and Eicken (1998).

3. RESULTS

3.1. General ice conditions

In February 1997, the ice extent in the Weddell Sea was rather high (Fig. 2), with highly deformed and thick ice in the southeast Weddell Sea (Haas and others, 1999; Table 2, shown later). The sampled floes were located across the entire Weddell Sea (Fig. 2), and were visited during a period of 42 days under varying climatic conditions (Fig. 3). Air temperatures measured on board *Polarstern* ranged between 0° and −5°C until day 55, when values dropped below −10°C when *Polarstern* transited a second time to the southeast, where minimum temperatures were as low as −22°C. However, at that location a slight cooling had already commenced by day 32, according to data logged by a drifting buoy in that region (Fig. 3b). The rather cold conditions started on day 49, about 7 days before the arrival of *Polarstern*. To distinguish between different climatic and ice regimes, the 1997 dataset is subdivided into three periods defined as summer (days 19–27) and early fall (days 56–61) in the southeast, and as summer in the northwest Weddell Sea (days 46–55; Figs 2 and 3). The 40° W meridian is taken as the boundary between the southeast and northwest Weddell Sea.

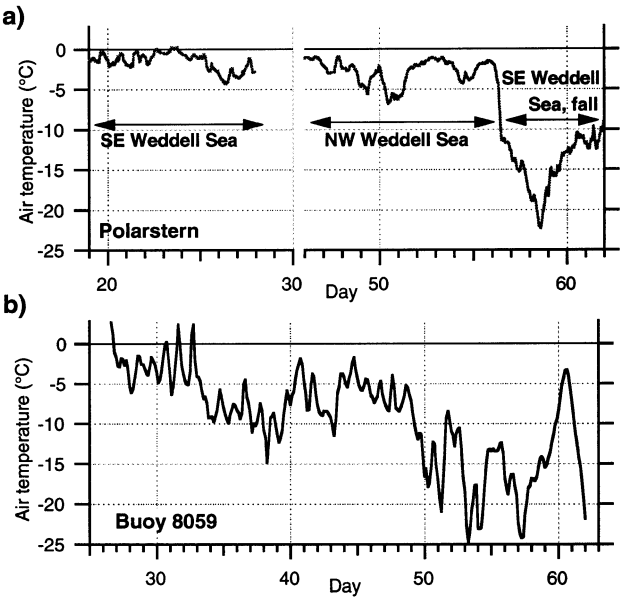

Fig. 3. Air temperatures recorded on board Polarstern *along the cruise track in 1997 (a) and by a drifting buoy (Argos ID 8059) at about 40° W, 73.2° S in the southeast Weddell Sea (b).*

In February 1994 in the Bellingshausen and Amundsen Seas, air temperatures ranged mostly between 0° and −4°C. Only close to the coast were lower temperatures (−5° to −8°C) encountered. With respect to ice thickness (Haas, 1998; Table 2, shown later), we distinguish between the Bellingshausen Sea and Amundsen Sea.

In late January 1997 (days 19–27) the ship operated in closed pack ice in the southeast Weddell Sea, with ice concentrations mostly higher than 0.9 and floe diameters up to 500 m. During the second phase of the expedition in the inner marginal ice zone floe sizes exceeded 100 m only on days 53 and 54 as well as 57 and 58, while ice concentration varied between 0.5 and 1.0. The ice in the northwest Weddell Sea was characterized by a mixture of thick deformed and thin level floes, indicating the presence of old and young ice, respectively (Lange and Eicken, 1991). The latter carried only a thin snow cover and their surfaces appeared greyish. In 1994, most floes were located well within the perennial ice zone (Haas and Viehoff, 1994; Morris and others, 1998), although their size was mostly <100 m.

Numerous surface ponds were observed throughout the southeast and northwest Weddell Sea, mostly originating from ridge loading (Ackley and Sullivan, 1994). However, aerial photographs (C. Haas, unpublished information) showed that they covered only 0.3% of the ice surface. The mean salinity of 19 pond-water samples was 19.4 ± 7.1 (range 8.3–30.9), indicating a mixture of sea water and melted snow and ice.

3.2. Snow properties

Table 1 summarizes the average snow thicknesses in each region calculated from the thickness-profile data of each floe. The snow layer was generally much thicker in the Bellingshausen and Amundsen Seas than in the Weddell Sea, where the thinnest snow was observed in the northwest. There, in contrast, winter observations of Eicken and others (1994) and Massom and others (1997) report the highest snow thicknesses of the Weddell Sea. Clearly, our findings indicate strong snowmelt in the northwest during summer, which will be discussed later in more detail.

Figure 4 shows typical vertical profiles of snow tempera-

https://doi.org/10.3189/172756501781831864 Published online by Cambridge University Press

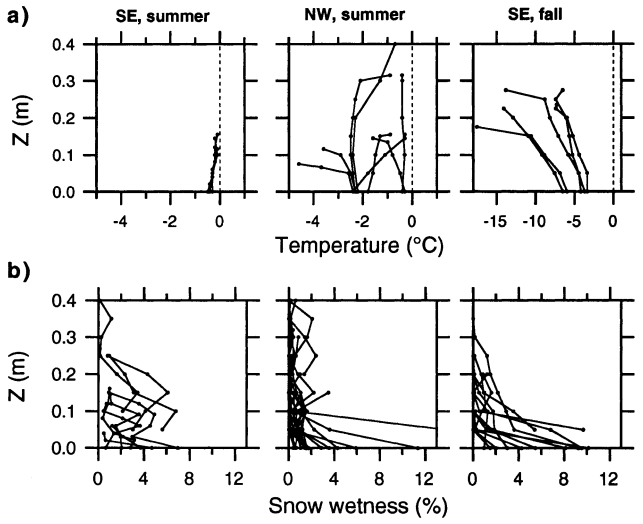

Fig. 4. Typical vertical snow profiles of (a) temperature obtained on level ice and (b) wetness (percentage liquid water by volume) obtained on level ice and ridge flanks in three different regions in 1997. Note different scale in upper right graph.

ture and wetness. The differences in air temperatures (Fig. 3) were clearly reflected in the snow (Fig. 4a). While temperatures in the southeast Weddell Sea were higher at the surface than at the snow/ice interface (positive gradients), positive as well as negative gradients were found in the northwest Weddell Sea. In both summer situations, temperatures at the snow/ice interface were close to or above the freezing point of sea water (−1.8°C). In contrast, strong negative gradients ranging from −8° to −66°C m^{-1} were observed in the southeast Weddell Sea in early fall, 75% of these being less than −25°C m^{-1}. Depth hoar was found in every snow pit. The ice surface had cooled below −5°C at several sites, and dendritic ice growth underneath the surface layer into the gap layer was observed (see below).

Figure 4b shows that snow wetness seldom exceeded 4% This means that during most of the sampling period the snow was in the pendular regime where liquid water cannot freely drain but is held at the triple junctions of ice grains and air. This regime promotes snow coarsening by the growth of grains into clusters. Snow wetness increased with depth on most floes and was highest at the bottom (Fig. 4b). This was most pronounced in the southeast Weddell Sea in fall.

Of all 169 salinity samples, only 31 had a salinity equal to or higher than 0.1‰ (Table 1). Only three samples which were obtained from the snow/ice interface had salinities higher than 1‰ in 1997. These summer values are significantly lower than measurements in other seasons, where mean snow salinities range between 1‰ and 16‰, with more than 10% of all measurements ranging from 10‰ up to 40‰ (Eicken and others, 1994; Massom and others, 1997; Sturm and others, 1998; Worby and others, 1998).

Snow density ranged between 130 and 518 kg m^{-3}, with means of 300–400 kg m^{-3}. Grain-sizes ranged between 1 and 10 mm, with mean values of 2.5–3.1 mm (Table 1). Apart from the depth hoar observed in the southeast Weddell Sea in fall, and fine new snow that mostly melted within 1 or 2 days, the snowpack consisted of coarse and very coarse grain clusters (seasonal-snow-on-the-ground classification 6cl/6mf; Colbeck and others, 1990). The snowpack was very icy at the bottom. Just above the snow/ice interface, grain-size increased rapidly and the grains were partially frozen onto the underlying ice. Therefore, the snow/ice interface was very rough on the centimetre scale. As the ice underneath was mostly superimposed ice (see below), the rough surface was a transition zone of snow being metamorphosed into ice.

Observed grain-sizes and densities are similar to values reported by others for snow which was subject to melting phases. However, they are much higher than values of cold Antarctic winter snow (Eicken and others, 1994; Massom and others, 1997; Sturm and others, 1998; Worby and others, 1998).

3.3. Ice properties

Table 2 summarizes all EM and drillhole thickness measurements. Note that these include both level and deformed ice, the fraction of the latter being rather high (Haas and others, 1999). The thickness of undeformed, level ice is 0.4–1.3 m (cf. Figs 5 and 6). However, mean thicknesses in the southeast Weddell Sea were much greater than those recorded in previously published winter data (Eicken and others, 1994; Massom and others, 1997), and are much closer to values reported by Strass and Fahrbach (1998). In the northwest Weddell Sea, thicknesses were comparable to those measured for undeformed second-year ice in spring in the same region (Lange and Eicken, 1991). The ice in the Bellingshausen and Amundsen Seas is some of the thickest Antarctic sea ice reported (Haas, 1998).

Table 1. Mean snow properties

	Southeast Weddell (summer)	*Northwest Weddell (summer)*	*Southeast Weddell (early fall)*	*Bellingshausen Sea*	*Amundsen Sea*
Snow thickness (m)	0.24 ± 0.02	0.11 ±0.14	0.20 ± 0.12	0.32 ± 0.16	0.51 ±0.11
Range	0.21–0.26	0.04–0.58	0.07–0.42	0.16–0.56	0.39 ± 0.75
N (floes)	5	14	10	9	10
Salinity (‰)	0.04 ± 0.09	0.17 ± 1.00	0.14 ± 0.45	0.02 ± 0.08	
Range	0–0.2	0–8.6 (1 sample >1)	0–2.4 (2 samples >1)	0–0.36 (3 samples > 0.1)	
N (samples)	5	81	46	37	
Density (kg m^3)	ND	368 ± 64	313 ± 72	391 ±71	
Range		218–480	130–496	212-518	
N (samples)		81	46	37	
Grain-size (mm)	ND	3.1 ±1.2	2.6 ± 1.2	2.5 ± 1.0	
Range		1–5.5	1–10.0	1–4.0	
N (samples)		81	46	11	

ND, not determined.

https://doi.org/10.3189/172756501781831864 Published online by Cambridge University Press

Table 2. Mean ice properties

	Southeast Weddell (summer) 11 floes	*Northwest Weddell (summer) 14 floes*	*Southeast Weddell (early fall) 8 floes*	*Bellingshausen Sea 6 floes*	*Amundsen Sea 9 floes*
Total thickness (m)	1.56 ± 0.31 (n = 5, EM)	1.52 ± 0.75 (n = 14, EM)	1.92 ± 1.39 (n = 8, EM)	2.37 ± 1.56 (n = 6, drilling)	5.11 ± 2.32 (n = 5, drilling)
Range	1.24–1.91	0.26–2.86	0.41–4.30	1.22–4.98	3.34–9.14
Freeboard	0.07 ± 0.05	0.08 ± 0.05	0.07 ± 0.05		
Range	0–0.14	0–0.17	0–0.13		
Percentage of gap features	73	86	38	ND	ND
Surface ice layer thickness (m)	0.07 ± 0.04	0.20 ± 0.06	0.15 ± 0.05	ND	ND
Range	0.02–0.15	0.10–0.29	0.10–0.16		
Surface layer draft (m)	0.02 ± 0.02	0.14 ± 0.05	0.14 ± 0.01	ND	ND
Range	0–0.07	0.08–0.23	0.13–0.15		
Gap thickness (m)	0.08 ± 0.09	0.04 ± 0.03	0.05 ± 0.06	ND	ND
Range	0.01–0.27	0.01–0.09	0.01–0.09		
PG ice thickness (m)	0.04 ± 0.03	0.08 ± 0.06	0.08 ± 0.01	0.10 ± 0.05	0.12 ± 0.07
Range	0–0.09	0.01–0.25	0.07–0.08	0.03–0.16	0.03–0.25
Texture classes (%)					
Orbicular granular	66	53	83	68	
Columnar	28	33	11	18	
PG	2	10	6	3	
Mixed/others	3	4	0	11	
PG ice salinity (‰)	0.68 ± 0.40	0.61 ± 1.06	3.78 ± 3.25	0.86 ± 1.26	

Notes: All listed variables except ice thickness were determined from surface or main ice cores. Texture classes derived from main ice cores only. Mean total thickness was calculated from EM and drillhole profiles.

ND, not determined.

Figure 5 shows high-resolution vertical cross-sections typical for floes encountered in the three ice regimes in the Weddell Sea, obtained from thickness drilling. While the floes in Figure 5a and c were rather level and much larger than 100 m, the floe in Figure 5b was only 40 m in diameter and comprised an old pressure ridge. All three profiles show the typical sequence of a snow layer above a surface ice layer overlying a slush- or sea-water-filled gap. Underneath, the main ice was encountered, which was often extremely rotten and porous (Figs 1 and 6b).

The frequency of occurrence, the thicknesses and drafts of the surface ice layers, as well as the gap thicknesses, are summarized in Table 2. In total, gap layers were observed on 64% of all 33 sampled floes in 1997. The surface ice layer in the southeast Weddell Sea was much thinner than in the other regions, and its underside was at or just below sea level (Fig. 5a; Table 2). This is similar to earlier summer observations of a crusty snow layer above the slush (Lytle and Ackley, 1996). Two samples of gap water had salinities of 14‰ and 17‰. In the other two regions, by contrast, the thick surface ice layer extended on average 0.14 m into the water, with most of its thickness not rising above the water level. The mean salinity of 37 gap-water samples was 29.3 ± 2.6‰ (range 20.6–31.3‰). As with the pond water, the low gap-water salinities indicate that melting was taking place within or adjacent to the gaps.

The lower portion of Figure 5a–c shows vertical profiles of texture and salinity of the main and some surface cores, as well as four δ^{18}O profiles. All cores consisted of superimposed PG ice at the top. The typical PG ice texture with isometric grains with planar boundaries can be seen in the thin- and thick-section photographs in Figure 6. Grain-size often decreased with depth. In the thick-section photographs (Fig. 6b and c), PG ice is less clearly recognizable once the grain-size becomes smaller than the sample thickness. Therefore, fractions of PG ice given below are probably underestimates of the real amount. The downward-decreasing grain-sizes also make it difficult to distinguish it from underlying fine-grained ice with higher salinities occurring in some instances (Figs 5 and 6). That ice is probably of snow-ice origin.

PG ice contributed significantly to the overall surface core lengths (see, e.g., Fig. 5b). It was found at the top of 76% of the 33 main cores taken in 1997, and of 73% of the 15 cores taken in 1994 (Fig. 2). Table 2 summarizes the mean PG ice-layer thicknesses. The smallest values occurred in the southeast Weddell Sea in summer; they doubled there by early fall. The greatest thicknesses were observed in the Bellingshausen and Amundsen Seas. The amount of PG ice growth during summer is roughly comparable with fractions of snow ice formed during flood–freeze cycles in the cold season (Eicken and others, 1994; Jeffries and others, 1997).

Figures 5 and 6 also show typical vertical high-resolution salinity and δ^{18}O profiles of the respective cores. Salinities of all surface and main cores are presented in Figure 7. They ranged between 3 and 4 for the main ice underneath the gap. In contrast, salinities were very low in the surface cores, and mostly zero for PG ice (Table 2). Only immediately above the gap were high salinities sometimes measured, coinciding with a fine-grained granular texture. Additionally, in some locations in the southeast Weddell Sea in fall, PG ice salinities rose at the top (see also Table 2), when the freeboard was less than about 0.01 m, or where the gap had started to refreeze. Then, the surface cores often revealed a C-shaped salinity profile (e.g. at 4 m in Fig. 5b), comparable to the salinity distribution of young nilas ice in winter. Apparently, ice formation within the gap leads to some upward brine expulsion.

The δ^{18}O values of the surface ice layers were extremely small (Figs 5 and 7). At the very top, they were more like values for snow, ranging between −3‰ and −28‰ in the Weddell Sea in winter (Eicken and others, 1994). With increasing depth, they slowly became more typical of sea ice, at 0–2.5‰, indicating the presence of snow ice (Eicken and others, 1994; Jeffries and others, 1997).

https://doi.org/10.3189/172756501781831864 Published online by Cambridge University Press

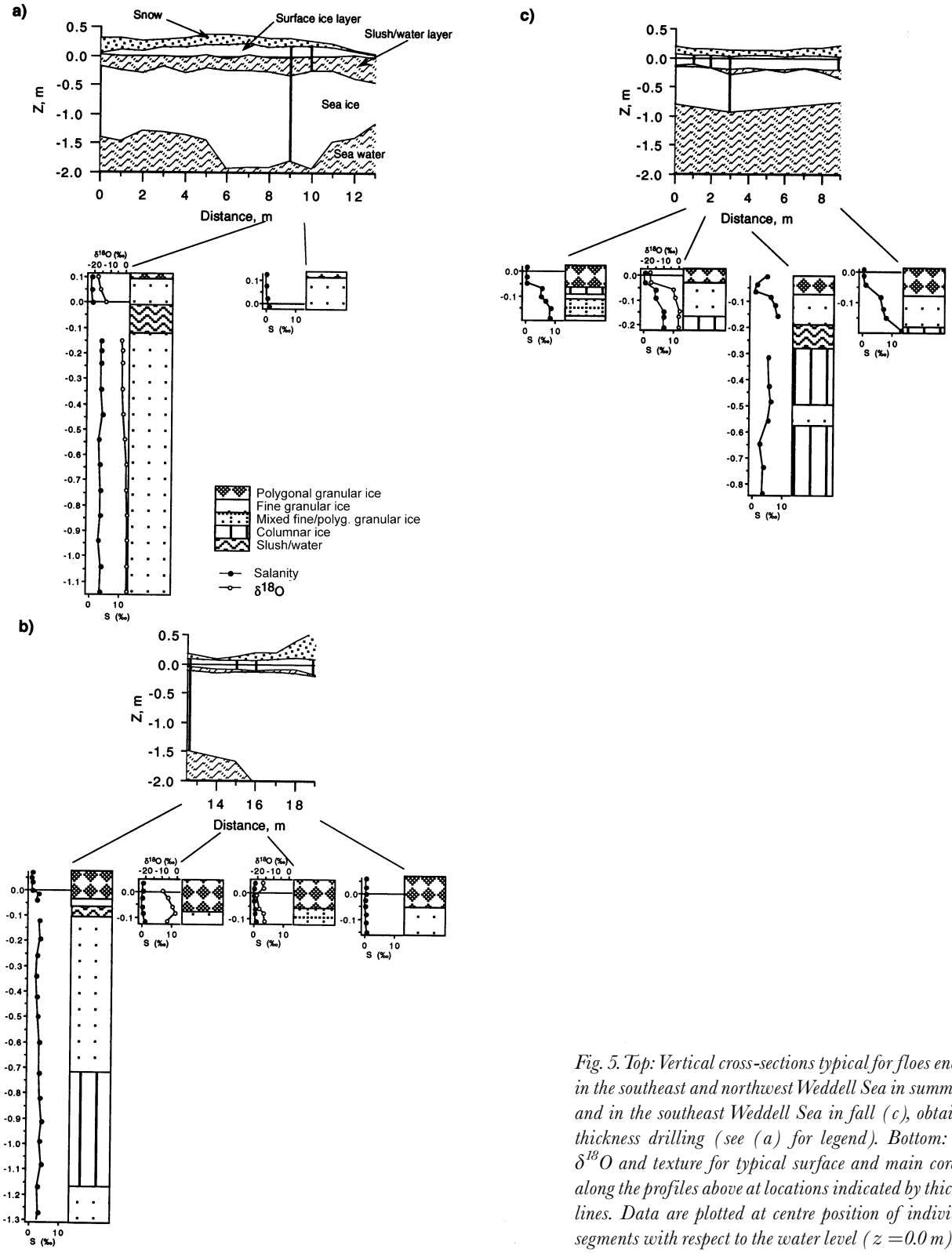

Fig. 5. Top: Vertical cross-sections typical for floes encountered in the southeast and northwest Weddell Sea in summer (a, b) and in the southeast Weddell Sea in fall (c), obtained from thickness drilling (see (a) for legend). Bottom: Salinity, $\delta^{18}O$ and texture for typical surface and main cores drilled along the profiles above at locations indicated by thick vertical lines. Data are plotted at centre position of individual core segments with respect to the water level ($z = 0.0$ m).

Two other common observations are worth mentioning (Fig. 6): First, PG ice was often underlain by a thin layer of columnar ice, either immediately below, as in Figure 6a, or further below, as in the case of dendritic new ice growing into the underlying gap (Fig. 6c). This columnar ice layer indicates the former presence of liquid water, in contrast to the fine-grained granular snow ice forming from slush during flood–freeze cycles. Secondly, in the southeast Weddell Sea in fall, surface ice with small freeboard often had a C-shaped salinity profile (Fig. 6b). Below the surface of this ice, salt-water droplets were observed within the fresh superimposed ice, indicating downward melting of sea water which had flooded the ice surface. The salt water caused the salinity increase at the top, and destroyed the PG texture of the ice, making the PG origin of the ice difficult to recognize. This observation was common on very rotten, thin ice, where the main sea ice underneath had melted almost completely and the floes consisted only of the surface ice layer (Fig. 6b). These features indicate the final stage of an ice floe in late summer, when it would either soon deteriorate completely or become restrengthened once subject to fall freezing. The rotten, highly porous structure of the ice underneath the gap (Fig. 6b) permits large convective transport of nutrients, salt and heat at the onset of fall freeze-up (Fritsen and others, 1994; Lytle and Ackley, 1996).

Finally, in Figures 5–7, note that PG and very low-salinity ice occurred below the water level. As this ice origi-

https://doi.org/10.3189/172756501781831864 Published online by Cambridge University Press

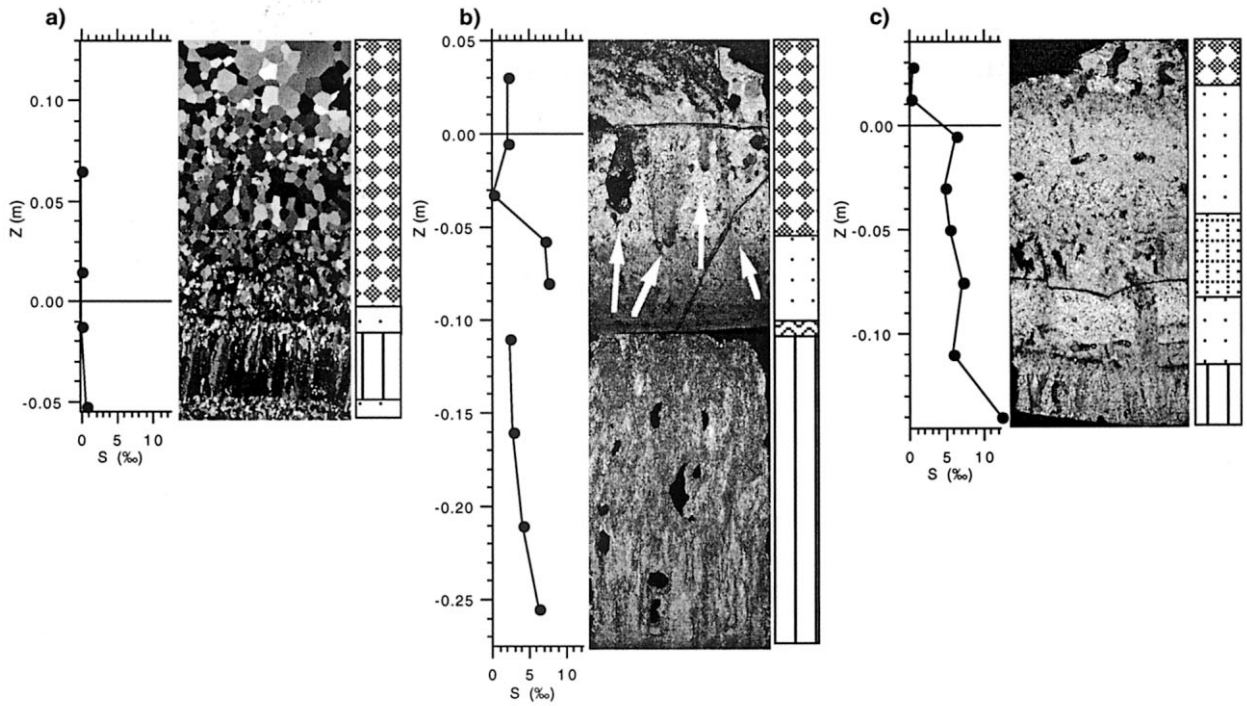

Fig. 6. Photographs of a thin section (a: 1994) and two thick sections (b, c: 1997) of three typical surface cores, taken with the samples between crossed polarizers. In addition, (b) shows the rotten ice between the gap and the bottom, and arrows mark salt-water droplets penetrating into the superimposed ice. The salinity profile of each core, plotted at the centre position of individual core segments with respect to the water level ($z = 0.0$ m, y axis), as well as the texture interpretation are also shown.

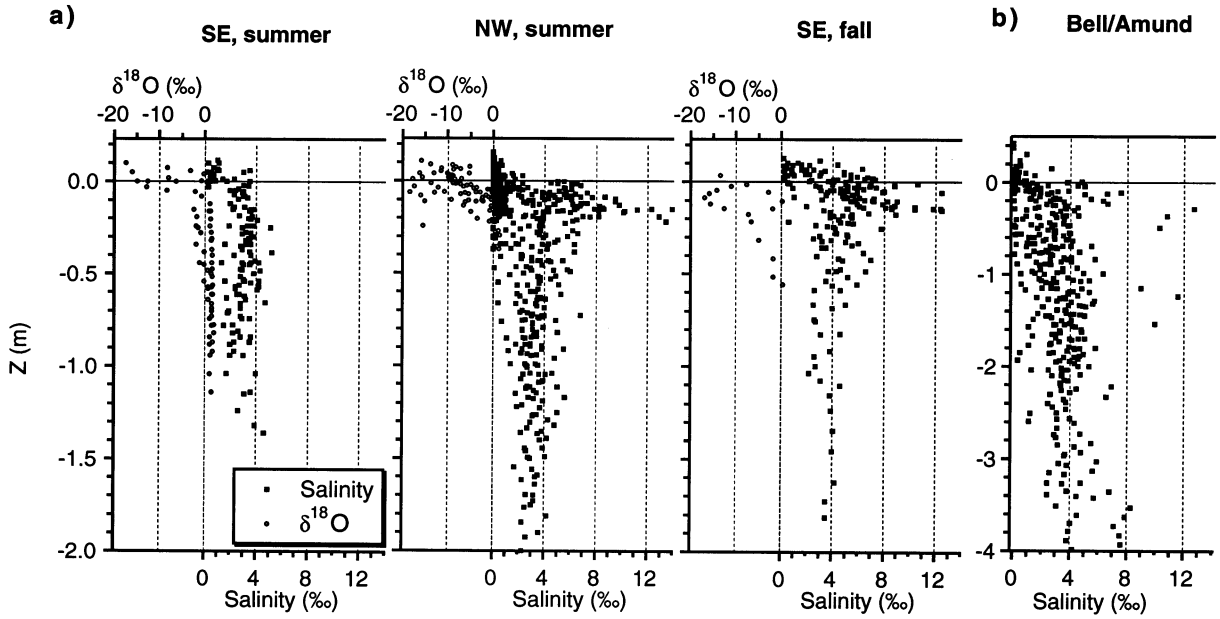

Fig. 7. Salinity and $\delta^{18}O$ profiles of all surface and main cores obtained in 1994 and 1997 plotted at centre position of individual core segments with respect to the water level ($z = 0.0$ m).

nated from the refreezing and metamorphosis of snow above sea level, it must have moved downward relative to the water level during summer.

Figure 8 presents chlorophyll-*a* concentrations of the upper metre of all cores obtained in the Weddell Sea. Unfortunately, the averaging over 0.1 m long segments does not allow detailed study of surface concentrations. However, it can be seen that chlorophyll-*a* concentrations were generally highest at 0.1–0.3 m depth below the surface, i.e. in the ice surrounding the gap. This demonstrates the importance of the surface-layer/gap structure for the primary productivity in perennially ice-covered regions. The highest concentrations of up to 439 $\mu g\,L^{-1}$ were found in the dendritic new ice forming from refreezing gaps in the southeast Weddell Sea in fall. Similar observations have been reported by Fritsen and others (1994).

4. DISCUSSION

4.1. Snowmelt and refreezing

We have presented numerous snow and ice data obtained from perennial Antarctic sea ice. Although the dataset is heterogeneous, several common features emerge which can be considered typical for the summer situation. Most importantly, there is considerable surface melting in the Antarctic

https://doi.org/10.3189/172756501781831864 Published online by Cambridge University Press

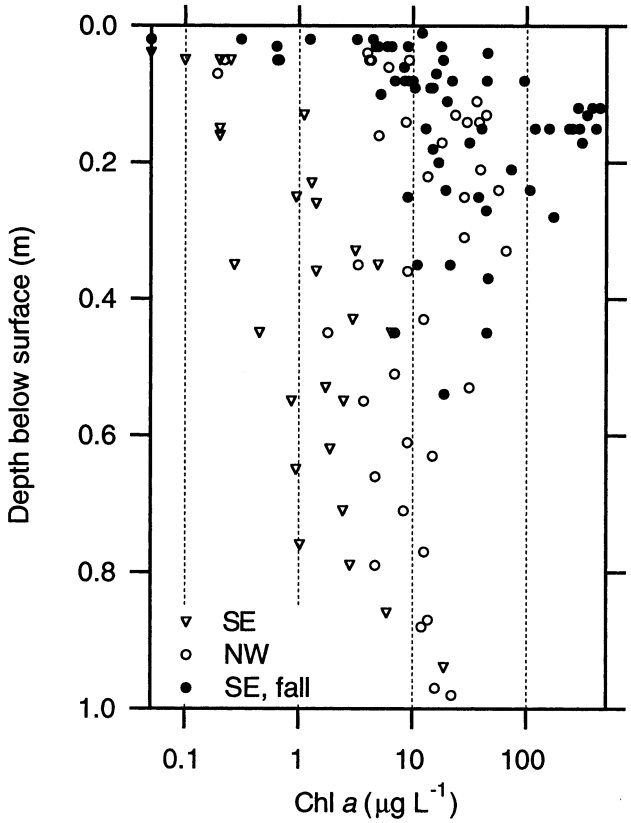

*Fig. 8. Chlorophyll-*a *concentrations of ice cores obtained in 1997, plotted at centre depth of individual core segments with respect to the ice surface. For clarity, data from below 1 m were omitted.*

pack ice. The amount of melt is much less than in the Arctic, where the snow melts completely and the ice surface is extensively covered with melt ponds. Nonetheless, internal snow melting on Antarctic sea ice is strong enough to induce extensive snow metamorphism and the formation of superimposed ice. In the northwest Weddell Sea, where the thickest snow occurs in winter, melting was strongest and resulted in both the thinnest residual snow cover and the thickest surface ice layer. Average superimposed ice thicknesses of 0.08–0.25 m correspond to late-winter snow thicknesses of 0.24–0.75 m if a snow density of 330 kg m^{-3} is assumed. The low snow salinities show that there was considerable meltwater percolation through the snow, transporting salt downwards. When measured, however, the snow was in the pendular regime. Nevertheless, there must have been episodic events of enhanced surface melt and percolation, for example during periods of warm-air advection (Massom and others, 1997; Morris and others, 1998). Snowmelt and wetness can also be much higher earlier in the season, when the amount of incoming solar radiation is highest. Very likely, wetness varies diurnally with changing solar elevation, resulting in melt–freeze cycling (Fig. 3b).

Although surface melting was regarded as atypical in earlier studies (Andreas and Ackley, 1982; Jeffries and others, 1994), the regional and temporal distribution of our observations and those of Fritsen and others (1994) and Lytle and Ackley (1996) suggests that it is actually quite common, not only in the marginal ice zone, but also within the inner pack.

Melting occurs even at air temperatures below 0°C through absorption of solar radiation within the snow (Colbeck, 1989; Launiainen and Cheng, 1998). Temperature gradients in a melting snowpack on sea ice are positive, i.e. temperatures decrease towards the ice surface, where they are close to the freezing point of sea water. This results in the refreezing of fresh meltwater further down at the snow/ice interface, and finally in the formation of superimposed ice with its PG texture. However, the measured low snow wetnesses could also indicate that superimposed ice may form just by growth and merging of grain clusters. The processes described have also been observed on Arctic fast ice (Holt and Digby, 1985; Onstott, 1992; Barber and others, 1998), although melting is much stronger there and more continuous. Therefore, the snow and successively the superimposed and underlying ice layers melt completely.

Generally, superimposed-ice formation should affect every spot of an ice floe, including level ice and pressure ridges. However, depending on the amplitude of melting and on the amount of meltwater, the water will drain to the lowest topographic parts of a floe where the thickest superimposed ice would then be formed. When melting is not strong enough to produce freely draining water, as indicated by our wetness measurements, lateral differences in the amount of superimposed-ice formation might be caused by heterogeneous snow properties. Clearly, the local variability in snow thickness, stratigraphy, grain types and iciness (Massom and others, 1997; Sturm and others, 1998) will result in different light penetration and scattering, causing variable intensities of internal melt.

4.2. Gaps

The other common summer feature is the widespread occurrence of slush- or water-filled porous layers or gaps underneath a surface ice layer. As outlined in the introduction, their origin has been explained as the result of summer warming and the subsequent increase in brine volume, which fosters a biophysical feedback mechanism (Ackley and others, 1979; Ackley and Sullivan, 1994). In fact, the high salinities near the top of first-year ice (Maykut and Untersteiner, 1971; Eicken, 1992) will result in large brine volumes once the ice warms up. However, the results of Zeebe and others (1996) show that a positive feedback mechanism by absorption of solar radiation would only be effective with rather high chlorophyll-*a* concentrations in the gap of >150 mg chl *a* m^{-2} and a snow cover thinner than 0.05 m. Although our snow and chlorophyll data suggest that absorption by algae might become significant in the course of the summer, these conditions are unlikely to prevail at the onset of summer warming. For example, Günther and Dieckmann (1999) observed no accelerated rise in nutrients or chlorophyll in the upper ice layers until the end of December in a time-series study on snow-covered fast ice.

However, the formation of gap layers can also be explained by purely abiotic processes. First, the widespread formation of snow-ice layers during flood–freeze cycles in the cold season provides a mechanism to form layered structures with strong salinity gradients (Fritsen and others, 1998; Maksym and Jeffries, 2000). Although some of the saline brine might be expelled downwards during flood–freeze events because the underlying ice is warm and permeable (Maksym and Jeffries, 2000), it is likely that some high-salinity layer remains at the former slush/ice interface on completion of the freeze cycle. These high saline layers would reopen as soon as ambient temperatures rise. As outlined by Eicken and others (1995) and Maksym and Jeffries (2000), due to energetic constraints, the slush layer will only incompletely congeal if

https://doi.org/10.3189/172756501781831864 Published online by Cambridge University Press

flooding and freezing commence after early September. Thus, there is a high probability that slush-filled gaps exist already at the end of winter. Where these are present, superimposed ice will form on top of snow ice overlying a gap, as shown in Figures 5 and 6.

Secondly, the surface-ice/gap structure might be formed due to melting of the snow above a slush layer of flooded snow. At negative freeboard, surface flooding is most probable and widespread in summer, as the ice is most permeable and the warm snow allows for long-range lateral flow of the sea water at the snow/ice interface. Initially, however, the temperature of the saline slush layer will be close to the freezing point of sea water. The less dense and fresh meltwater percolating through the overlying snow onto the cold slush surface will therefore refreeze at the interface, and will thicken by the addition and refreezing of more meltwater from above. The resulting structure was often observed in the southeast Weddell Sea in summer and is shown in Figure 5a. In this case, a snow-ice layer between the superimposed ice and the gap was missing (Figs 5a and b and 6a). The situation is comparable to the formation of ice below under-ice melt ponds in the Arctic (Eicken, 1994), where an ice layer forms at the boundary between a fresh- and a salt-water layer both at their freezing point.

Once the porous or gap layers have formed, the gaps are widened both by absorption of solar radiation and by advection of sea water from the floe edges. Absorption might be enhanced by high chlorophyll-*a* concentrations which could develop in the gap habitat once it had formed. Slight increases of the gap water temperature above its freezing point lead to melting of the slush within it or of the adjacent ice, as indicated by our gap-water salinity measurements. While in this case the gap water is diluted and might still be in phase equilibrium with its environment, advection of, and exchange with, more saline sea water from the floe edges leads to further melting, finally resulting in the rotten, honeycomb-like ice structure. This will be particularly important closer to the ice edge, where water motion within the floes can be induced by swell penetrating into the ice. Clearly, as also shown by nutrient data (e.g. Fritsen and others, 1994; Thomas and others, 1998), at the end of summer the permeability of the ice is high enough to allow for considerable exchange with the surrounding sea water. Another source of energy available for melting results from the downward flux of latent heat released by meltwater refreezing during superimposed-ice formation. As with the under-ice melt ponds, a small fraction of this heat is consumed by melting at the very bottom of the surface ice layer.

4.3. Summer surface processes

Our measurements were made while moving through both space and time. While the data from the southeast Weddell Sea represent conditions at the beginning of summer, the northwest Weddell Sea data are typical of the peak of the ablation season. As indicated by low air temperatures and the refreezing of gaps, measurements in the southeast Weddell Sea in fall show the transition back to winter conditions. By summarizing the observations in these regions, we suggest a heuristic model of processes on perennial Antarctic ice from late spring to early fall, shown in Figure 9.

The late-spring situation describes the preconditioning of the ice surface before the onset of surface melt. Freeboard is either positive (Fig. 9a) or negative. In the case of negative freeboard, flood–freeze cycling with the formation of snow ice may be present (Fig. 9c), or the snow may remain dry because the underlying ice is impermeable and flooding from the sides does not reach the interior of floes through the cold snow (Fig. 9b). Either way, the salinity at the top of the ice is high.

In summer, the ice and snow temperature gradients reverse. As a consequence, the porosity at the top of the ice increases drastically (Fig. 9a), incompletely frozen slush layers widen (Fig. 9c), or the ice surface becomes widely flooded (Fig. 9b). Simultaneously, snow metamorphoses and meltwater percolates downward, and superimposed ice forms above the water level, on top of either ice or slush. Generally, the summer season is also characterized by desalination of the original sea or snow ice below the gap. Among these processes, the "freeboard layer" mechanism (Ackley and others, 1979; Ackley and Sullivan, 1994) is just one possibility related to the porosity increase (Fig. 9a).

Finally, as air temperatures drop in fall, and snow and ice temperature gradients become negative again, superimposed-ice formation and widening of gaps cease. Depending on the amount of slush left in the gaps, they will congeal from top to bottom, developing either a columnar or granular texture. This final freezing, with all the consequences of high primary productivity and large vertical heat fluxes (Fritsen and others, 1994; Lytle and Ackley, 1996), concludes the summer season. Following continued accumulation of snow, the ice will begin to undergo the well-known processes of flood–freeze cycling.

4.4. Submergence

One more process complicates the transformations described above (Fig. 9): over summer, the ice slowly submerges further into the water due to changes in the isostatic equilibrium. First, during summer the ice melts from below. Depending on the amount of ocean heat flux and on the initial ice thickness, a thinning of 0.2–0.6 m can occur during summer (Martinson and Iannuzzi, 1998). Secondly, mass is added as either snow or rain to the ice surface. According to data presented by Eicken and others (1994), snow accumulation from December to February amounts to 0.12–0.16 m at the continental coast of the southeast Weddell Sea, and is much higher in the northwest. Finally, submergence is also due to internal melt, leading to increased brine volumes and therefore higher bulk densities. While density increases of 10–20 kg m^{-3} are possible (based on calculations using the equations of Cox and Weeks (1983)) for warming of the ice to close-to-melting temperatures, even higher bulk density rises are likely for the ice–water mixture of the very rotten, honeycomb-like ice.

The amount of submergence in relation to changes in these variables can easily be deduced by differentiating the equation for ice freeboard z_{fb}

$$z_{\mathrm{fb}} = z_{\mathrm{i}} - [\rho_{\mathrm{i}}(z_{\mathrm{i}} + \rho_{\mathrm{s}})z_{\mathrm{s}}]/\rho_{\mathrm{water}} \qquad (1)$$

for snow and ice thickness z_{s} and z_{i}, as well as for ice density ρ_{i}. Characteristic values are given in Table 3. As can be seen, the three variables in total could yield submergence distances of >0.1 m during the summer months. Thus, drafts of the surface ice layer of 0.14 m (Table 2) can be explained by submergence alone, if the superimposed ice has formed immediately above a slush layer. On the other hand, as

https://doi.org/10.3189/172756501781831864 Published online by Cambridge University Press

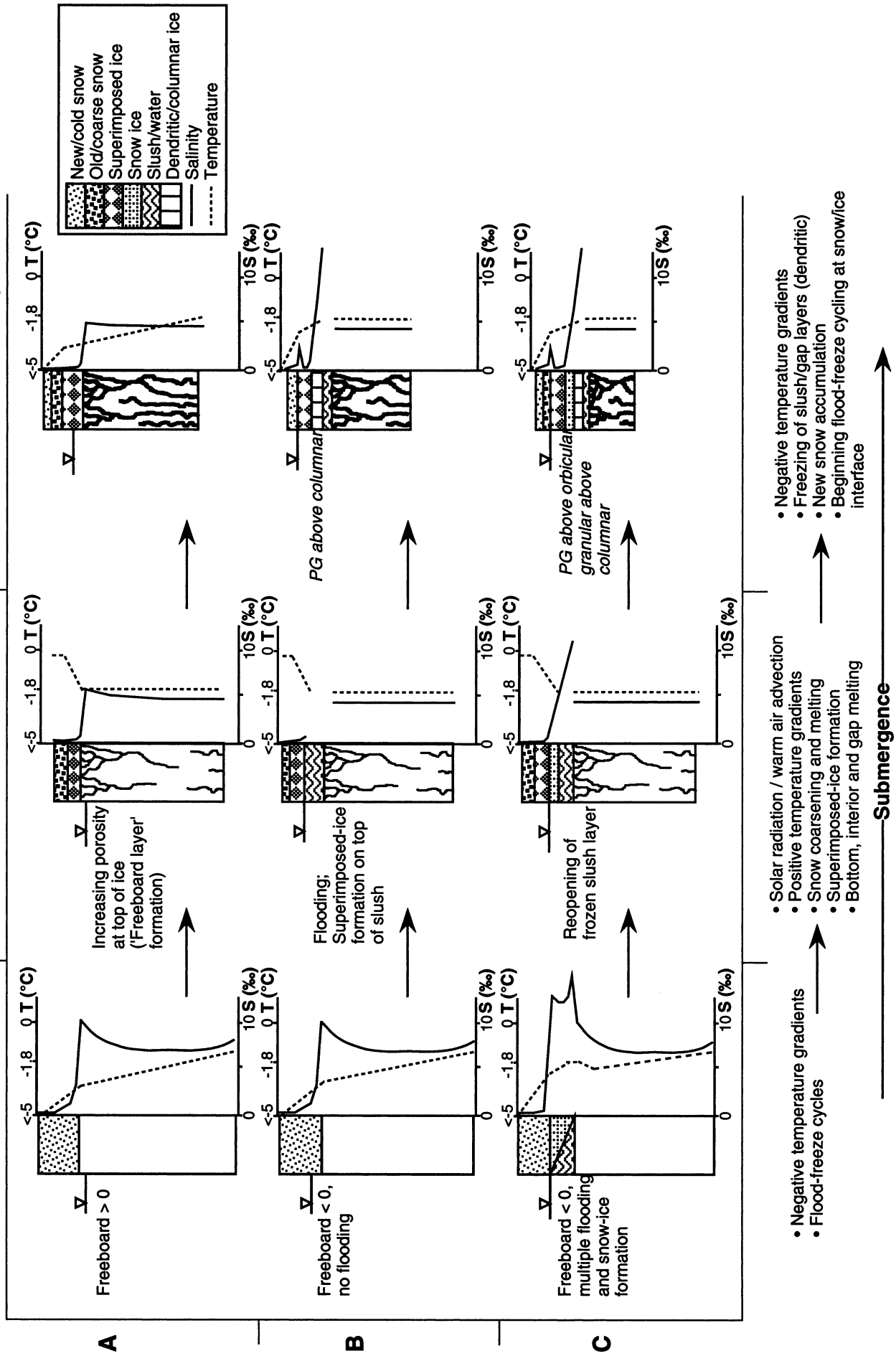

Fig. 9. Schematic drawing of summer surface processes described in the text.

https://doi.org/10.3189/172756501781831864 Published online by Cambridge University Press

Table 3. Sensitivity of ice freeboard $\mathrm{d}z_{\mathrm{fb}}$ *to changes in ice and snow thickness* $\mathrm{d}z_{\mathrm{i}}$ *and* $\mathrm{d}z_{\mathrm{s}}$ *and in ice density* $\mathrm{d}\rho_{\mathrm{i}}$*, as calculated by differentiating Equation (1) for each respective variable*

Ice thickness z_{i} ($\rho_{\mathrm{i}} = 920\,\mathrm{kg\,m^{-3}}$)		*Snow thickness* z_{s} ($\rho_{\mathrm{s}} = 350\,\mathrm{kg\,m^{-3}}$)		*Ice density* ρ_{i} ($z_{\mathrm{i}} = 0.5\,\mathrm{m}$)		($z_{\mathrm{i}} = 1\,\mathrm{m}$)	
$\mathrm{d}z_{\mathrm{i}}$	$\mathrm{d}z_{\mathrm{fb}}$	$\mathrm{d}z_{\mathrm{s}}$	$\mathrm{d}z_{\mathrm{fb}}$	$\mathrm{d}\rho_{\mathrm{i}}$	$\mathrm{d}z_{\mathrm{fb}}$	$\mathrm{d}\rho_{\mathrm{i}}$	$\mathrm{d}z_{\mathrm{fb}}$
m	m	m	m	$\mathrm{kg\,m^{-3}}$	m	$\mathrm{kg\,m^{-3}}$	m
−0.2	−0.02	0.1	−0.03	20	−0.01	20	−0.02
−0.4	−0.04	0.15	−0.05	30	−0.01	30	−0.03
−0.6	−0.06	0.2	−0.07	40	−0.02	40	−0.04

Note: For all calculations, a water density of $1024\,\mathrm{kg\,m^3}$ has been assumed.

explained earlier, the gaps may form already at some depth below the water level.

The data presented in Figures 5–7 show that the low surface ice salinities and δ^{18}O ratios are not changed much when the ice submerges. However, once freeboard becomes very small or even negative, as in Figures 5c and 6b, flooding might again take place, either causing a new cycle or ending superimposed-ice formation completely at the end of summer. Then, salinities at the very top are raised and eventually salt-water droplets may melt themselves into the superimposed ice, destroying the original PG texture (Fig. 6b). Thus, during summer there is a competition between upward superimposed-ice formation and downward ice submergence. Ultimately, the latter takes over towards the end of the ablation season unless it is balanced by ice growth at the ice underside.

Internal snowmelt and superimposed-ice formation will take place both in the perennial and in the seasonal ice zone. In the latter, however, submergence and surface flooding are so strong that no significant amounts of superimposed ice can form above the water level even before new flooding takes place and the ice finally deteriorates.

5. CONCLUSIONS

We have presented ice-core and salinity data obtained from perennial Antarctic sea ice during summer. The data show the widespread occurrence of snow metamorphosis and superimposed-ice formation on drifting pack ice. We have also discussed the formation of sea-water-filled gaps typical for summer sea ice. Both features are linked to each other only indirectly, although both are generally related to a thick snow cover. As a prerequisite, temperature gradients have to reverse in the snow and ice compared to the cold season. Our results reveal that submergence, well known to occur during the cold season and manifested in the extensive formation of snow ice, continues during summer. Thus, throughout the year, the behaviour of sea ice in the Antarctic is opposite to that of its counterpart in the Arctic Basin, where the ice generally rises upwards by bottom freezing in winter and surface melting in summer. While summer ice formation mainly takes place at the underside of Arctic ice by freezing of under-ice ponds, ice grows only at the surface in Antarctica.

Superimposed-ice formation is important in many respects. First, no mass is removed from the ice surface by run-off even if snow melts. This, and the thermodynamic consequences of melting and refreezing for the energy balance, have to be considered in numerical modelling studies. In contrast, snowmelt then contributes to summer ice formation. Second, the resulting layer is mechanically very strong, and extends the lifetime of a particular floe by preventing fracturing and deterioration of the otherwise rotten ice. Therefore, for example, solar radiation input into the upper water layer is reduced. The low-salinity, superimposed-ice layer floats in water with sub-freezing temperatures, thus melting only slowly. Third, the transformation of light-scattering snow into clear, well-transmitting ice considerably changes the optical properties of the ice surface. This and the coarsening of snow reduces the albedo, as was obvious from the greyish appearance of many floes.

Although we lack quantitative data of surface roughness and porosity of superimposed ice, the fresh, bubbly ice along with the coarse snow in the pendular regime will strongly increase radar backscatter. This is well known from the Arctic (Holt and Digby, 1985; Onstott, 1992). Around Antarctica also, Drinkwater (1998) and Morris and others (1998), for example, show higher radar backscatter of perennial ice in summer than in winter. Haas (2001) links the seasonal cycle of European Remote-sensing Satellite scatterometer signatures with the summer processes discussed here. Rapid increases of backscatter between November and December mark the onset of superimposed-ice formation. This increase is sporadically interrupted by sudden signal drops indicating stronger melt events and snow wetting. The slow signal decline from March onwards corresponds to the transition to flood–freeze cycle processes. Thus, radar backscatter can be taken to distinguish between warm- and cold-season regimes. The seasonal backscatter cycle is observed in all perennially ice-covered regions around Antarctica, showing the widespread occurrence of the processes described here.

By increasing light transmission and supporting the persistence of sea-water-filled gaps, the surface ice layer is of great importance for establishing high biological activity, and in particular high algal standing stocks within summer sea ice (Fig. 8). In fact, these particular ice habitats support the greatest biological activities in pack ice recorded in the Southern Ocean, comparable to those found in land-fast bottom ice or platelet assemblages (Thomas and others, 1998). Our heuristic model links the physical processes leading to several habitats formerly described by others. In fact, it appears that the infiltration layers (Syvertsen and Kristiansen, 1993), as well as the highly porous or "freeboard layers" (Ackley and others, 1979; Garrison and Buck, 1991; Ackley and Sullivan, 1994; Fritsen and others, 1994, 1998) observed between late spring and early fall, correspond to specific stages of the processes outlined here. Thus, the gap layers (summer B and C in Fig. 9) might well have developed from superimposed-ice formation on top of what was an infiltration layer before (late-spring B in Fig. 9).

Our observations are biased by problems with sampling rotten summer ice, and by the thick-section analyses. The former leads to the loss of brine from the ice, on the one hand, and the contamination of fresh ice with salt water, on the other. The latter problem results in underestimates of the amount of superimposed PG ice, which cannot easily be distinguished from granular snow ice if the grain-size is small. However, the low salinity and δ^{18}O of much of the fine-grained ice shows that it also is solely of meteoric origin. The question whether superimposed-ice formation is a continuous, diurnal or episodic event could not be answered, as the measured snow wetness was relatively low. Although we introduced abiotic processes for the initial formation of gap layers, the role of biophysical feedback mechanisms in further developing these features remains unclear and deserves quan-

https://doi.org/10.3189/172756501781831864 Published online by Cambridge University Press

tification. Therefore, more detailed and quantitative future studies of summer processes are a challenge to sampling methods and strategies. This would also require the permanent monitoring of transformations in ice properties and of the meteorological and oceanographic forcing at fixed locations (e.g. at a drift station during melt onset).

ACKNOWLEDGEMENTS

We would like to express our sincere gratitude to captains and crews as well as to the scientific cruise leaders H. Miller and W. Jokat of RV *Polarstern* during ANT 11/3 and ANT 14/3 for their support of our work. Sampling also benefited greatly from the care and companionship of the helicopter teams. J. Askne kindly lent us the snow fork. M. Steffens helped in the field. Constructive reviews by S. Gerland and S. Ackley, as well as editorial remarks by M. Sturm, improved the paper considerably. We also acknowledge discussions with G. Dieckmann and H. Eicken. The work was partly supported by the Nuffield Foundation, U.K. Natural Environment Research Council (GT9/2894, GR9/3309) and the Deutscher Akademischer Austauschdienst/British Council (ARC Programme).

REFERENCES

Ackley, S. F. and C.W. Sullivan. 1994. Physical controls on the development and characteristics of Antarctic sea ice biological communities — a review and synthesis. *Deep-Sea Res., Ser. I*, **41** (10), 1583–1604.

Ackley, S. F., K. R. Buck and S. Taguchi. 1979. Standing crop of algae in the sea ice of the Weddell Sea region. *Deep-Sea Res.*, **26** (3), 269–281.

Andreas, E. L. and S. F. Ackley. 1982. On the differences in ablation seasons of Arctic and Antarctic sea ice. *J. Atmos. Sci.*, **39** (2), 440–447.

Barber, D. G., A. Thomas and T. N. Papakyriakou. 1998. Role of SAR in surface energy flux measurements over sea ice. *In* Tsatsoulis, C. and R. Kwok, *eds. Analysis of SAR data of the polar oceans: recent advances*. Berlin, etc., Springer-Verlag, 35–67.

Colbeck, S. C. 1987. Theory of particle coarsening with a log-normal distribution. *Acta Metall.*, **35** (7), 1583–1588.

Colbeck, S. C. 1989. Snow-crystal growth with varying surface temperatures and radiation penetration. *J. Glaciol.*, **35** (119), 23–29.

Colbeck, S. C. 1997. A review of sintering in seasonal snow. *CRREL Rep.* 97-10.

Colbeck, S. C. *and 7 others*. 1990. *The international classification for seasonal snow on the ground*. Wallingford, Oxon, International Association of Scientific Hydrology. International Commission on Snow and Ice.

Cox, G. F. N. and W. F. Weeks. 1983. Equations for determining the gas and brine volumes in sea-ice samples. *J. Glaciol.*, **29** (102), 306–316.

Drinkwater, M. R. 1998. Active microwave remote sensing observations of Weddell Sea ice. *In* Jeffries, M. O., *ed. Antarctic sea ice: physical processes, interactions and variability*. Washington, DC, American Geophysical Union, 187–212. (Antarctic Research Series 74.)

Drinkwater, M. R. and C. Haas. 1994. *Snow, sea-ice, and radar observations during ANT X/4: summary data report*. Bremerhaven, Alfred Wegener Institute for Polar and Marine Research. Physics Department. (Report 53.)

Eicken, H. 1992. Salinity profiles of Antarctic sea ice: field data and model results. *J. Geophys. Res.*, **97** (C10), 15,545–15,557.

Eicken, H. 1994. Structure of under-ice melt ponds in the central Arctic and their effect on the sea-ice cover. *Limnol. Oceanogr.*, **39** (3), 682–694.

Eicken, H. 1998. Deriving modes and rates of ice growth in the Weddell Sea from microstructural, salinity and stable-isotope data. *In* Jeffries, M. O., *ed. Antarctic sea ice: physical processes, interactions and variability*. Washington, DC, American Geophysical Union, 89–122. (Antarctic Research Series 74.)

Eicken, H. and M. A. Lange. 1989. Development and properties of sea ice in the coastal regime of the southeastern Weddell Sea. *J. Geophys. Res.*, **94** (C6), 8193–8206.

Eicken, H., M. A. Lange, H.-W. Hubberten and P. Wadhams. 1994. Characteristics and distribution patterns of snow and meteoric ice in the Weddell Sea and their contribution to the mass balance of sea ice. *Ann. Geophysicae*, **12** (1), 80–93.

Eicken, H., H. Fischer and P. Lemke. 1995. Effects of the snow cover on Antarctic sea ice and potential modulation of its response to climate change. *Ann. Glaciol.*, **21**, 369–376.

Fritsen, C. H., V. I. Lytle, S. F. Ackley and C.W. Sullivan. 1994. Autumn bloom of Antarctic pack-ice algae. *Science*, **266** (5186), 782–784.

Fritsen, C. H., S. F. Ackley, J. N. Kremer and C.W. Sullivan. 1998. Flood–freeze cycles and microalgal dynamics in Antarctic pack ice. *In* Lizotte, M. P. and K. R. Arrigo, *eds. Antarctic sea ice: biological processes, interactions and variability*. Washington, DC, American Geophysical Union, 1–21. (Antarctic Research Series 73.)

Garrison, D. L. and K. R. Buck. 1991. Surface-layer sea ice assemblages in Antarctic pack-ice during austral spring: environmental conditions, primary production and community structure. *Mar. Ecol. Prog. Ser.*, **75**, 161–172.

Gloersen, P., W. J. Campbell, D. J. Cavalieri, J. C. Comiso, C. L. Parkinson and H. J. Zwally. 1992. *Arctic and Antarctic sea ice, 1978–1987: satellite passive-microwave observations and analysis*. Washington, DC, National Aeronautics and Space Administration. (NASA SP-511.)

Gow, A. J., S. F. Ackley, K. R. Buck and K. M. Golden. 1987. Physical and structural characteristics of Weddell Sea pack ice. *CRREL Rep.* 87-14.

Günther, S. and G. Dieckmann. 1999. Seasonal development of high algal biomass in snow-covered fast ice and the underlying platelet layer in Atka Bay, Antarctica. *Antarct. Sci.*, **11** (3), 305–315.

Haas, C. 1998. Evaluation of ship-based electromagnetic-inductive thickness measurements of summer sea-ice in the Bellingshausen and Amundsen Seas, Antarctica. *Cold Reg. Sci. Technol.*, **27** (1), 1–16.

Haas, C. 2001. The seasonal cycle of ERS scatterometer signatures over perennial Antarctic sea ice and associated surface ice properties and processes. *Ann. Glaciol.*, **33**, 69–73.

Haas, C. and T. Viehoff. 1994. Sea ice conditions in the Bellingshausen/Amundsen Sea: shipboard observations and satellite imagery during ANT XI/3. *Alfred-Wegener-Inst. für Polar- und Meeresfors., Bremerhaven, Germany, Tech. Rep.* 51.

Haas, C., H. Rebhan, D. N. Thomas and T. Viehoff. 1996. Sea ice. *In* Miller, H. and H. Grobe, *eds. The Expedition ANTARKTIS-XI/3 of RV Polarstern* in 1994. Bremerhaven, Alfred Wegener Institute for Polar and Marine Research, 29–43. (Report 188/96.)

Haas, C., S. Gerland, H. Eicken and H. Miller. 1997. Comparison of sea-ice thickness measurements under summer and winter conditions in the Arctic using a small electromagnetic induction device. *Geophysics*, **62** (3), 749–757.

Haas, C., D. N. Thomas, M. Steffens and J. Bareiss. 1998. Physical and biological investigations of sea ice. *In* Jokat, W. and H. Oerter, *eds. The Expedition ANTARKTIS-XV of RV Polarstern* in 1997: report of leg ANT-XIV/3. Bremerhaven, Alfred Wegener Institute for Polar and Marine Research, 18–30. (Report 267/96.)

Haas, C., Q. Liu and T. Martin. 1999. Retrieval of Antarctic sea-ice pressure ridge frequencies from ERS SAR imagery by means of in-situ laser profiling and usage of a neural network. *Int. J. Remote Sensing*, **20** (15–16), 3111–3123.

Holt, B. and S. A. Digby. 1985. Processes and imagery of first-year fast sea ice during the melt season. *J. Geophys. Res.*, **90** (C3), 5045–5062.

Jeffries, M. O. and W. F. Weeks. 1993. Structural characteristics and development of sea ice in the western Ross Sea. *Antarct. Sci.*, **5** (1), 63–75.

Jeffries, M. O., R. A. Shaw, K. Morris, A. L. Veazey and H. R. Krouse. 1994. Crystal structure, stable isotopes (δ^{18}O), and development of sea ice in the Ross, Amundsen, and Bellingshausen seas, Antarctica. *J. Geophys. Res.*, **99** (C1), 985–995.

Jeffries, M. O., A. P. Worby, K. Morris and W. F. Weeks. 1997. Seasonal variations in the properties and structural composition of sea ice and snow cover in the Bellingshausen and Amundsen Seas, Antarctica. *J. Glaciol.*, **43** (143), 138–151.

Kawamura, T., K. I. Ohshima, S. Ushio and T. Kakizawa. 1993. Sea-ice growth in Ongul Strait, Antarctica. *Ann. Glaciol.*, **18**, 97–101.

Kawamura, T., K. I. Ohshima, T. Takizawa and S. Ushio. 1997. Physical, structural and isotopic characteristics and growth processes of fast sea ice in Lützow–Holm Bay, Antarctica. *J. Geophys. Res.*, **102** (C2), 3345–3355.

Kottmeier, S. T. and C. W. Sullivan. 1990. Bacterial biomass and production in pack ice of Antarctic marginal ice edge zones. *Deep-Sea Res., Ser. A*, **37** (8), 1311–1330.

Lange, M. A. 1988. Basic properties of Antarctic sea ice as revealed by textural analysis of ice cores. *Ann. Glaciol.*, **10**, 95–101.

Lange, M. A. and H. Eicken. 1991. The sea ice thickness distribution in the northwestern Weddell Sea. *J. Geophys. Res.*, **96** (C3), 4821–4837.

Lange, M. A., S. F. Ackley, P. Wadhams, G. S. Dieckmann and H. Eicken. 1989. Development of sea ice in the Weddell Sea. *Ann. Glaciol.*, **12**, 92–96.

Lange, M. A., P. Schlosser, S. F. Ackley, P. Wadhams and G. S. Dieckmann. 1990. ^{18}O concentrations in sea ice of the Weddell Sea, Antarctica. *J. Glaciol.*, **36** (124), 315–323.

Launiainen, J. and B. Cheng. 1998. Modelling of ice thermodynamics in natural water bodies. *Cold Reg. Sci. Technol.*, **27** (3), 153–178.

Lytle, V. I. and S.F. Ackley. 1996. Heat flux through sea ice in the western Weddell Sea: convective and conductive transfer processes. *J. Geophys. Res.*, **101** (C4), 8853–8868.

Maksym, T. and M. O. Jeffries. 2000. A one-dimensional percolation model

of flooding and snow-ice formation on Antarctica sea ice. *J. Geophys. Res.*, **105**(C11), 26,313–26,331.

Martinson, D. G. and R. A. Iannuzzi. 1998. Antarctic ocean–ice interaction: implications from ocean bulk property distributions in the Weddell Gyre. *In* Jeffries, M. O., *ed. Antarctic sea ice: physical processes, interactions and variability.* Washington, DC, American Geophysical Union, 243–271. (Antarctic Research Series 74.)

Massom, R. A., M. R. Drinkwater and C. Haas. 1997. Winter snow cover on sea ice in the Weddell Sea. *J. Geophys. Res.*, **102**(C1), 1101–1117.

Maykut, G. A. and N. Untersteiner. 1971. Some results from a time-dependent thermodynamic model of sea ice. *J. Geophys. Res.*, **76**(6), 1550–1575.

Morris, K., M. O. Jeffries and S. Li. 1998. Sea ice characteristics and seasonal variability of ERS-1 SAR backscatter in the Bellingshausen Sea. *In* Jeffries, M. O., *ed. Antarctic sea ice: physical processes, interactions and variability.* Washington, DC, American Geophysical Union, 213–242. (Antarctic Research Series 74.)

Onstott, R. 1992. SAR and scatterometer signatures of sea ice. *In* Carsey, F. D. *and 7 others, eds. Microwave remote sensing of sea ice.* Washington, DC, American Geophysical Union, 73–104. (Geophysical Monograph Series 68.)

Sihvola, A. and M. Tiuri. 1986. Snow fork for field determination of the density and wetness profiles of a snow pack. *IEEE Trans. Geosci. Remote Sensing*, **GE-24**(5), 717–721.

Strass, V. H. and E. Fahrbach. 1998. Temporal and regional variation of sea ice draft and coverage in the Weddell Sea obtained from upward looking sonars. *In* Jeffries, M. O., *ed. Antarctic sea ice: physical processes, interactions and variability.* Washington, DC, American Geophysical Union, 123–139. (Antarctic Research Series 74.)

Sturm, M., K. Morris and R. Massom. 1998. The winter snow cover of the West Antarctic pack ice: its spatial and temporal variability. *In* Jeffries, M. O., *ed. Antarctic sea ice: physical processes, interactions and variability.* Washington, DC, American Geophysical Union, 1–18. (Antarctic Research Series 74.)

Syvertsen, E. E. and S. Kristiansen. 1993. Ice algae during EPOS, leg 1: assemblages, biomass, origin and nutrients. *Polar Biol.*, **13**(8), 61–65.

Thomas, D. N. *and 7 others.* 1998. Biological soup within decaying summer sea ice in the Amundsen Sea, Antarctica. *In* Lizotte, M. P. and K. R. Arrigo, *eds. Antarctic sea ice: biological processes, interactions and variability.* Washington, DC, American Geophysical Union, 161–171. (Antarctic Research Series 73.)

Worby, A. P. and I. Allison. 1999. A technique for making ship-based observations of Antarctic sea ice thickness and characteristics. Part I. Observational techniques and results. *Antarct. CRC Res. Rep.* 14, 1–23.

Worby, A. P., R. A. Massom, I. Allison, V. I. Lytle and P. Heil. 1998. East Antarctic sea ice: a review of its structure, properties and drift. *In* Jeffries, M. O., *ed. Antarctic sea ice: physical processes, interactions and variability.* Washington, DC, American Geophysical Union, 41–67. (Antarctic Research Series 74.)

Zeebe, R. E., H. Eicken, D. H. Robinson, D. Wolf-Gladrow and G. S. Dieckmann. 1996. Modelling the heating and melting of sea ice through light absorption by microalgae. *J. Geophys. Res.*, **101**(C1), 1163–1181.

MS received 20 March 2000 and accepted in revised form 16 August 2001

https://doi.org/10.3189/172756501781831864 Published online by Cambridge University Press